3D LINE RECONSTRUCTION FROM AIRBORNE THREE-LINE SCANNER DATA

Sander Oude Elberink[*] and George Vosselman
Faculty of Civil Engineering and Geosciences
Department of Geodesy, Section of Photogrammetry and Remote Sensing
Delft University of Technology
S.J.Oude-Elberink@mdi.rws.minvenw.nl, G.Vosselman@geo.tudelft.nl

ABSTRACT:

This paper deals with the automatic reconstruction of 3D object lines from airborne three-line scanner data. These novel sensor systems contain three linear CCD arrays which are oriented perpendicular to the flight direction of the aircraft. In a first processing step, raw image data is projected onto a plane at mean terrain height, resulting in three so-called rectified images with different viewing angles. Although these images are visually equal to frame images, after rectification they still contain small projection errors due to aircraft movements in combination with the line perspective geometry of the sensor. We present a new two-step feature-based approach to extract 3D information from three-line scanner data. In the first step 2D extracted lines are matched in three rectified images. Due to errors in the rectified images and in the 2D line extraction, the matching algorithm only provides approximate 3D information. After the approximate alignment of the object line by the matching algorithm, more precise estimates of pose parameters can be obtained by a least squares fitting algorithm in the second step. In this step the geometry of the recording situation is used in order to remove projection errors. Results of the two-step approach are shown for a complex building model, proving the high potential of airborne digital line scanners for 3D feature extraction purposes.

1. INTRODUCTION

Automatic extraction of 3D information from multiple 2D images is one of the most challenging problems in computer vision research. When dealing with airborne imaging, the challenge adresses to the reconstruction of man-made objects like buildings or even complete city models. Those models may be used in applications such as virtual reality, tele-presence, digital cinematography and urban planning (Stamos and Allen, 2000). Many (semi-) automatic reconstruction methods have been published for object reconstruction from aerial images, for example [Sahar and Krupnilc, 1999], [Henricsson and Baltsavias, 1997] and [Vosselman and Veldhuis, 1999]. These methods are based on analogue aerial images, which were digitised with an high resolution scanner.

An important step towards fully automatic object reconstruction is to use digital instead of analogue images. Recently, high-resolution digital image data with stereo capabilities has become available with the arrival of airborne three-line scanners, like the HRSC-A (High Resolution Stereo Camera – Airborne) (Wewel et al, 1999) and the ADS40 (Airborne Digital Sensor) (Fricker and Walker, 2000). These sensor systems consist of a focal plane with three linear CCD arrays that are oriented perpendicular to the flight direction of the aircraft. As a result of the aircraft motion this configuration generates stereo imagery by scanning the terrain surface strips (pushbroom principle). The advantages of using airborne three-line scanner compared to normal frame images are the high radiometric resolution of 16 bits, three-view stereo configuration, and direct availability of digital image data. The major disadvantages are the weak geometry of line scanner data and limited geometric resolution. In order to use the advantages and minimise the disadvantages of line scanner data, a new reconstruction method has to be built-up.

A characteristic of man-made objects is the presence of straight object lines. Therefore, our object reconstruction relies on a line-based approach: extracted lines in 2D are matched in three images to reconstruct object lines in 3D. The three-view matching configuration is expected to be more accurate and reliable in comparison to normal two-view stereo configuration.

Section 2 describes the properties of the line scanner used in our research: the ADS40 from LH-systems. The paper follows with the steps of 3D line reconstruction: line extraction and approximate reconstruction by matching (section 3), refinement of the approximate alignment by a fitting algorithm (section 4). Conclusions of the developed method are presented in section 5.

2. GEOMETRY OF THE SENSOR

Thanks to recent developments in CCD sensor technology and GPS/INS integration, airborne digital cameras are able to produce images with a ground resolution below 25 centimeter. High radiometric resolution (8-16 bits) and multispectral properties of these digital sensors may result in better interpretation and segmentation of the acquired scene compared to normal analogue images. Because line scanners have a different perspective geometry than frame images, a further look at the geometric properties is necessary.

---

[*] At the moment of appearance of this paper the author is working at the Survey Department of the Ministry of Transport, Public Works and Water Management, Delft, The Netherlands.

Three panchromatic sensor lines of the three-line scanner produce forward, nadir and backward views along the strip. The three lines, each consisting of an CCD array of 12.000 pixels, lie in the focal plane, perpendicular to the flying direction. Unlike frame photography, where all pixels in the image are exposed simultaneously, each line of a line scanner image is collected in a pushbroom fashion at a different instant of time (Lee et al, 2000). To be able to relate pixels in raw line scanner images to coordinates in an orthogonal ground coordinate system, the interior and exterior orientations have to be known. The interior orientation parameters (x, y, f) relate each CCD pixel to the projection centre, where (x, y) is the position of the lens centre in the focal plane and f is the focal length. The exterior orientation parameters (X, Y, Z, ω, φ, κ), which have to be known at any exposure (200 Hz), describe the position and rotation of the sensor coordinate system with respect to the ground coordinate system.

The six parameters of the exterior orientation have been determined by integration of GPS measurements (Global Positioning System) and INS measurements (Inertial Navigation System). In a so-called IMU (Inertial Measurement Unit) the high-frequency INS data (>200 Hz) is updated every second by GPS measurements. Interpolation of these data to every exposure provides the exterior orientation parameters per scan line. Ground coordinates can be obtained by projecting the sensor pixels on a plane at a certain height level Z_0.

$$\begin{pmatrix} X \\ Y \\ Z_0 \end{pmatrix}_{ground} = \lambda R(\varphi, \omega, \kappa) \begin{pmatrix} x \\ y \\ -f \end{pmatrix} + \begin{pmatrix} X \\ Y \\ Z \end{pmatrix}_{platform} \quad [1]$$

Figure 1 shows the appearance of a building in the nadir view before and after rectification. At a flying height of 3000 meters the ground resolution of the ADS40 is 25 cm.

If we compare the characteristics of the rectified images with those of normal frame images, three major differences can be found:
1. Objects in rectified line scanner images are subject to a line perspective relief displacement whereas in frame images the relief displacement is central perspective.
2. During acquisition of an object the line scanner moves forward, resulting in various projection centres, i.e. resulting in various projections of one and the same object line. If the sequence of the projection centres does not form a horizontal straight line, the projection of a straight object line will not be a straight line. In frame images the central projection of a straight 3D object line is always a straight 2D line (assuming no lens distortions).
3. Aircraft movements between two stereo viewings result in a non-epipolar geometry. Because the distortions are less than the pixel size it is

possible to reconstruct a stereo model from two rectified images which is visually correct. From a mathematical point of view it can be shown that

Figure 1: Raw nadir image data (upper), rectified nadir image (lower).

height determination from rectified line scanner images is erroneous.

Due to the line perspective geometry, most of the object lines are recorded at several exposures, and are actually represented by a sequence of discrete points. To examine the behaviour of a straight object line in rectified images, a closer look at relief displacement of these points is necessary. Relief displacements of single points can be split up in along track and across track displacements. Most interesting is the across track displacement, which reads:

$$dy = \frac{(y_{pc} - y_{obj})}{(h_{pc} - h_{obj})} \cdot h_{obj}. \quad [2]$$

H_{pc}, h_{obj} is the flying height respectively the object height above projection plane, $(y_{pc}-y_{obj})$ is the across track distance between airplane and object. The maximum distance between the curved projected line and a virtual straight line between the two end points, depends on object height above projection plane and the side looking angle, and can be formulated by :

$$\Delta dy = \frac{1}{2}(dy_{end1} + dy_{end2}) - dy_{middle} =$$

$$\frac{1}{2} \cdot \left(\frac{(y_{pc} - y_{obj})}{(h_{pc} - h_{obj})} \cdot h_{obj} + \frac{(y_{pc} - (y_{obj} + \Delta y_{obj}))}{(h_{pc} - (h_{obj} + \Delta h_{obj}))} \cdot (h_{obj} + \Delta h_{obj}) \right)$$ [3]

$$- \frac{(y_{pc} - (y_{obj} + \frac{\Delta y_{obj}}{2}))}{(h_{pc} - (h_{obj} + \frac{\Delta h_{obj}}{2}))} \cdot (h_{obj} + \frac{\Delta h_{obj}}{2})$$

Δh_{obj} , Δy_{obj} is the height difference respectively the across track difference of the object line. It can easily be seen that if Δh_{obj} equals zero, Δdy becomes zero. This means that line perspective geometry does not distort straight horizontal lines. Slanted and vertical straight object lines will not be projected as straight lines, but will show a curve in rectified images. Distortion can exceed the ground pixel size, especially when slanted lines lie at large across track distance.

Besides these distortions, aircraft movements are another source of errors. The size of projection errors due to aircraft movements in relation to a straight horizontal line can be approximated by:

$$\Delta dy = \left(\frac{\Delta y_{pc}}{h_{pc} - h_{obj}} + \frac{-\Delta h_{pc} \cdot (y_{pc} - y_{obj})}{(h_{pc} - h_{obj})^2} \right) \cdot h_{obj}$$ [4]

With Δy_{pc} , Δh_{pc} horizontal and vertical aircraft movements. Typical error sizes due to aircraft movements vary between 0 and 5 centimeter. Programs working with sub-pixel precision, like line extraction and matching algorithms, will be influenced by these distortions.

The larger the difference between the reference plane and object height the larger the error of the pixel position in the rectified image (Börner et al, 1997). This difference has negative influences on the extraction of 2D and 3D geo-information. In order to minimise these errors, height information is needed. Height information can be determined by a matching algorithm (section 3). Because the matching is based on erroneous rectified images, the extracted 3D information has to be refined in an iterative method (section 4).

3. APPROXIMATE OBJECT RECONSTRUCTION

Straight lines that are characteristic for man-made objects will appear as (almost) straight lines in the rectified images. They are extracted by grouping adjacent pixels with similar gradient direction and fitting a straight line with sub-pixel precision through these pixels. Often this leads to fragmented line segments or multiple line segments representing one object line (Oude Elberink, 2001).

For 3D object reconstruction straight line segments at object edges need to be matched between at least two overlapping views. To speed up the searching of corresponding line segments, two constraints have been applied:

1. Given a line segment *l* in the first view, line segment *l'* in the second view must have a nonempty intersection with the image region between two straight lines in flight direction through the endpoints of *l*. This is comparable to the modified epipolar constraint for line segments in frame images described in [Bignone et al, 1996], [Suveg and Vosselman, 2000] and [Scholze et al, 2000]. The overlapping part of the line segments will be used for further computations.

2. Two images are needed to produce 3D information. Acquiring a scene using a three-line scanner will lead to three overlapping views, providing two independent stereo configurations. The third image gives us the opportunity to formulate a constraint to the matching: direction and height of the two independent 3D lines have to coincide with eachother within in a certain tolerance. The approximate position of the object line has been determined by averaging the two 3D lines.

Due to fragmentation in the 2D line extraction, the reconstructed 3D object lines are fragmented as well. The fragmentation even increases in 3D due to the property that only the overlapping part of three extracted lines will be reconstructed. One 2D extracted line can thus be cut in more than one 3D line segments.

For computational reasons the 3D lines are represented by six Plücker coordinates (v_x, v_y, v_z, u_x, u_y, u_z), similar to (Förstner, 2000).

$$L = \bar{v} + \mu \bar{u} .$$

$$\bar{v} \cdot \bar{u} = 0 \Leftrightarrow v_x u_x + v_y u_y + v_z u_z = 0.$$

$$\|\bar{u}\| = 1 \Leftrightarrow \sqrt{u_x^2 + u_y^2 + u_z^2} = 1.$$

[5],[6],[7]

The lines are defined by a positioning vector (v_x, v_y, v_z) through the origin and a direction vector (u_x, u_y, u_z) perpendicular to the positioning vector, see figure 2. The second condition, to get four degrees of freedom for an infinite 3D line, is the normalisation of the direction vector.
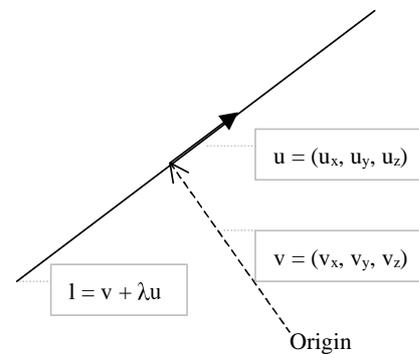
u = (u_x, u_y, u_z)

v = (v_x, v_y, v_z)

l = v + λu

Origin

Figure 2: Infinite 3D line represented in Plücker coordinates.

4. REFINEMENT OF THE RECONSTRUCTION

In order to remove the projection errors and its negative influences on the 2D and 3D reconstruction, we use the height information to project raw data on a local plane through the 3D object line. As one can see in section 2 the projection errors become zero when Δh (h_{obj}-h_{plane}) is zero.

When an object line is recorded, high grey value gradients occur in the image data, due to the reflectance properties of (the surrounding of) the edge of the object. This physical property is now used in order to refine the reconstructed object line. Raw image pixels whose rays cross the approximated object line within a certain distance, are expected to have recorded (the surrounding of) the 3D object line. (A ray is the line starting from the CCD element through the projection centre, see figure 3.) The refinement consist of an adjustment of the 3D line such that the line is determined by high gradient pixels, in nadir, forward and backward configuration. This optimisation criterion can be established by least squares minimisation of the perpendicular distances between rays of high gradient pixels and the 3D line. This has been done by weighting the distance with the
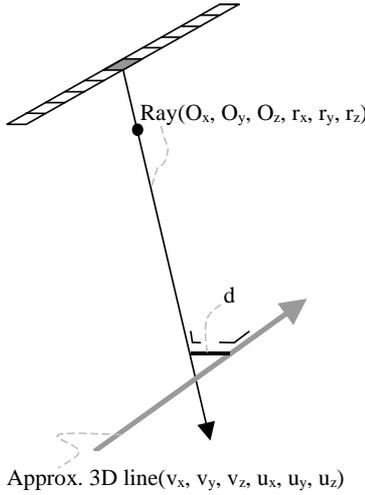

Figure 3: Geometric configuration of observation (d).

grey value gradient, perpendicular to the 3D line. The effect of the weights is that the estimation of the 3D line is dominated by rays through edges of the reconstructed object.

The perpendicular distance d between a ray and the 3D line can be written as:

$$d = \frac{u \times r}{\|u \times r\|} \cdot (v - O) = s'(v - O), \qquad [8]$$

$$\text{with } s' = \frac{s}{\|s\|}, \text{ and } s = u \times r.$$

For all rays within some distance of the approximate 3D line the observation equations are introduced. The meaning of using observation equations is that it expresses the distance d in terms of the unknown changes to the parameters of the 3D object line Δp_i.

$$E\{d\} = \sum_{i=1}^{i=n} \frac{\partial d}{\partial p_i} \Delta p_i, \quad W\{d\} = \left(\frac{\partial g}{\partial d}\right)^2. \; [9]$$

Where $E\{d\}$ denotes that d is expected to be equal to the linear expression at the right-hand side of the equation, and $W\{d\}$ is the weight of the observed distance. The elements $\partial d / \partial p_i$ are the partial derivatives of distance d to the object line parameters and can be written in terms of the approximate 3D object line and the ray elements.

$$\frac{\partial d}{\partial X_v} = X_{S'}, \qquad\qquad [10]$$

$$\frac{\partial d}{\partial Y_v} = Y_{S'}, \qquad\qquad [11]$$

$$\frac{\partial d}{\partial Z_v} = Z_{S'}, \qquad\qquad [12]$$

$$\frac{\partial d}{\partial X_u} = \frac{\frac{\partial s}{\partial X_u} - s'(s' \cdot \frac{\partial s}{\partial X_u})}{\|s\|} \cdot (v - O),$$
$$[13]$$

$$\text{with } \frac{\partial s}{\partial X_u} = \begin{pmatrix} 0 \\ -Z_r \\ Y_r \end{pmatrix}$$

$$\frac{\partial d}{\partial Y_u} = \frac{\frac{\partial s}{\partial Y_u} - s'(s' \cdot \frac{\partial s}{\partial Y_u})}{\|s\|} \cdot (v - O),$$
$$[14]$$

$$\text{with } \frac{\partial s}{\partial Y_u} = \begin{pmatrix} Z_r \\ 0 \\ -X_r \end{pmatrix}$$

$$\frac{\partial d}{\partial Z_u} = \frac{\frac{\partial s}{\partial Z_u} - s'(s' \cdot \frac{\partial s}{\partial Z_u})}{\|s\|} \cdot (v - O),$$
$$[15]$$

$$\text{with } \frac{\partial s}{\partial Z_u} = \begin{pmatrix} -Y_r \\ X_r \\ 0 \end{pmatrix}$$

For each 3D line, the observation equations are put in a model of observation equations. For m observed distances d, the model can be represented as follows:

$$E\begin{Bmatrix} d_1 \\ \cdot \\ \cdot \\ d_m \end{Bmatrix} = \begin{pmatrix} a_{11} & \cdot & a_{1n} \\ \cdot & \cdot & \cdot \\ \cdot & \cdot & \cdot \\ a_{m1} & \cdot & a_{mn} \end{pmatrix} \begin{pmatrix} \Delta p_1 \\ \cdot \\ \cdot \\ \Delta p_n \end{pmatrix} ;$$

$$\begin{pmatrix} b_{11} & \cdot & b_{1n} \\ b_{21} & \cdot & b_{2n} \end{pmatrix} \begin{pmatrix} \Delta p_1 \\ \cdot \\ \cdot \\ \Delta p_n \end{pmatrix} = \begin{pmatrix} 0 \\ 0 \end{pmatrix} ; \qquad [16]$$

$$W\begin{Bmatrix} d_1 \\ \cdot \\ \cdot \\ d_m \end{Bmatrix} = \begin{pmatrix} w_1 & & 0 \\ & & \\ & & \\ 0 & & w_m \end{pmatrix}$$

Simplifying [16] gives:

$$\mathrm{E}\{d\} = A\Delta p \,; \; B^*\Delta p = 0 \,; \; W\{d\} \qquad [17]$$

Where A is a (m by n)- matrix containing the partial derivatives for all observations, and B^* is a (2 by n)-matrix to ensure that the two Plücker conditions from equations [6] and [7] are fulfilled after updating the parameters, and W is the weighting matrix.

By least squares minimisation of the distance d, weighted by the gradients, the solution leads to the corrections to the parameters of the object line. The parameters of the object line are updated in an iterative process:

$$p_i^{(k+1)} = p_i^{(k)} + \Delta\hat{p}_i^{(k)} \qquad [18]$$

Representation [17] is in the form of observation equations with conditions on the parameter vector. Now the least squares solution can be obtained in a two-step calculation:

$$1 \; \Delta\hat{p}_A = (A^*WA)^{-1} A^*Wd \qquad [19]$$

$$2 \; \Delta\hat{p} = [I - Q_{\Delta\hat{p}_A} B (B^* Q_{\Delta\hat{p}_A} B)^{-1} B^*]\Delta\hat{p}_A,$$

$$\text{with } Q_{\Delta\hat{p}_A} = (A^*WA)^{-1}. \qquad [20]$$

In the first step one considers equation [17] without the conditions on the parameters. In the second step the temporary solution is projected from the R^6 space into the R^4 space, restricting the six parameter values such that the updated 3D line $p^{(k+1)}$ fulfils the two Plücker conditions. As one can see in figure 4 the fitting algorithm fits line segments to the strongest edge, shown for nadir data (raw image pixels projected on local plane).

Visually the succes of the algorithm can best be seen in figure 5: fragmented 3D lines representing one object line converge to one optimal solution. The accuracy of the reconstruction of the object lines after matching is about 50-60 centimeter in horizontal and 100 centimeter in vertical direction and after fitting about 15 centimeter in horizontal and 25 centimeter in vertical direction. So, the fitting algorithm increases

the accuracy of the reconstructed object lines with a factor between 3 and 4.
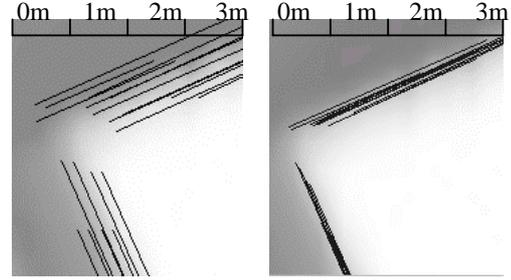

Figure 4: Fitting to strongest edge: matched line segments (left), back projected fitted line segments (right).
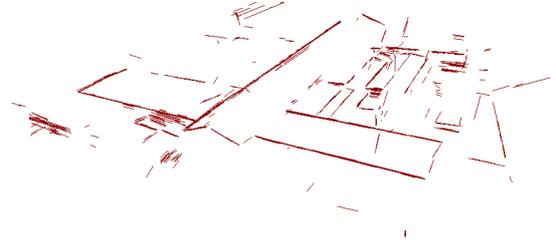

Figure 5: 3D view on the fitted line segments.

5. CONCLUSIONS

The use of digital data instead of analogue images is a major step towards fully automatic object reconstruction. Three-line scanners proof to produce suitable data for automatic 3D line reconstruction. This suitability is expressed in high geometric and radiometric resolution, together with the reliability of a triple viewing angle. The line perspective geometry causes distortions in the rectified images, which depend on the object height above the projection plane. Height information can be obtained by matching corresponding features in all three images. Most of the mismatches in the two-view stereo configuration are removed when using three viewing angles. When using rectified images, feature-based matching algorithms produce 3D lines, which still contain errors. We proposed to use the geometry of the recording situation in a least squares fitting step in order to remove these errors, finally resulting in accurate 3D line equations. Fitting results showed the convergence of fragmented reconstructed lines to one object line. The automatic reconstruction of 3D object lines shows the potential of airborne digital sensors to reconstruct complete object models in a fully automatic approach.

6. REFERENCES

Bignone, F., O. Henricsson, P. Fua, M. Stricker, "Automatic extraction of generic house roofs from

high resolution aerial imagery." In *Proceedings of 4th European Conference on Computer Vision*, pp. 85-96, Cambridge, 1996.

Börner, A., R. Reulke, M. Scheele, T. Terzibaschian, "Stereo processing of image data from an airborne three-line CCD scanner*." Presented at the Third International Airborne Remote Sensing Conference and Exhibition*, Copenhagen, 7-10 July 1997.

Förstner, W., "New orientation procedures." *International Archives of Photogrammetry and Remote Sensing*, Vol XXXIII, part B3, pp. 297-304, Amsterdam, 2000.

Fricker, P. and S. Walker, "Photogrammetry goes totally digital". *GIM International*, Vol 14 (8), pp. 54-57, 2000.

Lee, C., H. Theiss, J. Bethel, E. Mikhail, "Rigorous mathematical modeling of airborne pushbroom imaging systems". *Photogrammetric Engineering & Remote Sensing*, Vol. 66(4), pp. 385-392, 2000.

Oude Elberink, S., "Line matching and fitting in three-line scanner data". *Presented at the Fifth International Airborne Remote Sensing Conference*, San Francisco, California, 17-20 September, 2001.

Sahar, L. and A. Krupnilc, "Semiautomatic extraction of building outlines from large-scale aerial image". *Photogrammetric Engineering & Remote Sensing*, Vol. 65(4), pp. 459-465, 1999.

Scholze, S., T. Moons, F. Ade, L. van Gool, "Exploiting color for edge extraction and line segment stereo matching in high-resolution aerial imagery." *International Archives of Photogrammetry and Remote Sensing*, Vol. XXXIII, part B3, pp. 815-822, Amsterdam, 2000.

Stamos, I. and P. Allen, "3-D Model Construction using range and image data", *Proceedings of the IEEE Conference on Computer Vision and Pattern Recognition*, Vol. 1, pp. 531-536, 2000.

Suveg, I., G. Vosselman "3D reconstruction of building models*." International Archives of Photogrammetry and Remote Sensing*, Vol XXXIII, part B2, pp. 538-545, Amsterdam, 2000.

Vosselman, G. and H. Veldhuis, "Mapping by dragging and fitting of wire-frame models." *Photogrammetric Engineering & Remote Sensing* 65(7), pp. 769-776, 1999.

Wewel, F., F. Scholten, K. Gwinner. High Resolution Stereo Camera (HRSC) – Multispectral data acquisition and photogrammetric data processing. *Presented at the Fourth International Airborne Remote Sensing Conference and Exhibition*, Ottawa, Ontario, Canada, 21-24 June, 1999.

7. ACKNOWLEDGEMENTS